Estimation of primary production in the southern Argentine continental shelf and shelf-break regions using field and remote sensing data

CrossMark

A.I. Dogliotti [a,b,*], V.A. Lutz [c,d], V. Segura [c]

[a] Instituto de Astronomía y Física del Espacio (IAFE), CONICET-UBA, Pabellón IAFE-Ciudad Universitaria, C.C. 67-Suc. 28, C1428ZAA Ciudad Autónoma de Buenos Aires, Argentina
[b] Instituto Franco–Argentino para el Estudio del Clima y sus Impactos (UMI IFAECI/CNRS-CONICET-UBA), Ciudad Universitaria Pabellón II Piso 2, C1428EHA Ciudad Autónoma de Buenos Aires, Argentina
[c] Instituto Nacional de Investigación y Desarrollo Pesquero (INIDEP), Paseo Victoria Ocampo No. 1, B7602HSA Mar del Plata, Argentina
[d] Instituto de Investigaciones Marinas y Costeras, Consejo Nacional de Investigaciones Científicas y Técnicas (CONICET), Argentina

ARTICLE INFO

ABSTRACT

The Argentine continental shelf and shelf-break regions comprise a large and rich biological area of the ocean. However, field estimations of primary production are scarce, making remote sensing of ocean color a valuable tool to provide synoptic maps of primary production in this ecologically relevant region. Field studies performed during spring 2005, and summer and winter 2006 showed a high spatial and seasonal variability in the daily integrated water column primary production, chlorophyll-a and biomass-normalized photosynthetic parameters. Using field measurements, five different and relatively simple (non-spectral and vertically homogeneous biomass) models were tested: three chlorophyll-, one carbon- and one absorption-based model. The chlorophyll-based 'BIOM' model developed by Platt and Sathyendranath (*Science*, 241:1613–1620, 1988) provided the closest estimates to the field values, and was selected as the local algorithm. Its performance was assessed using simultaneous satellite-derived products and field photosynthetic parameters as input. Close values compared to the field estimates were obtained using BIOM (Absolute Percent Difference error, APD ~10%), even though satellite-derived products used as input to the model (i.e. chlorophyll-*a* concentration, diffuse attenuation coefficient in the photosynthetically active radiation range — PAR-, and PAR irradiance) showed relative high errors (APD ~40%, 20% and 50%, respectively). Provided that an efficient way to assign the physiological parameters in a pixel-by-pixel basis is found, this model seems to be the best to produce primary production maps from remote sensing of ocean color in the southern Argentine shelf and shelf-break regions.

1. Introduction

The Argentine continental shelf is one of the widest and flattest continental shelves in the world ocean; it widens southward from 170 km at 38°S to about 800 km at 50°S. It is a highly dynamic region characterized by the confluence of two western boundary currents (Brazil and Malvinas currents) and the presence of several oceanographic fronts; the shelf-break front between shelf subantarctic waters and Malvinas Current waters (Martos & Piccolo, 1988) and several tidal fronts which develop in spring and summer that define the border between vertically mixed and stratified shelf waters. These frontal areas have been associated with enhanced chlorophyll concentration (Carreto, Carignan, Montoya, & Cuchi-Colleoni, 2007; Rivas, Dogliotti, & Gagliardini, 2006; Romero, Piola, Charo, & Garcia, 2006) and with intense CO_2 uptake from spring through autumn (Bianchi et al., 2009). A negative correlation between sea–air partial pressure difference and chlorophyll concentration

(*Chla*, symbols used in the text are summarized in Table 1) over the shelf was found and photosynthesis was suggested as one of the main processes responsible for the large CO_2 sequestration (Bianchi et al., 2009). The high productivity in this region sustains commercially important species of fish and mollusks which develop their life cycle in connection to the different frontal areas (Bertolotti, Brunetti, Carreto, Prenzki, & Sánchez, 1996), sea birds and marine mammals (Campagna, Quintana, Le Boeuf, Blackwell, & Crocker, 1998). Despite its ecological and biogeochemical relevance, there are scarce field measurements of phytoplankton primary production (El-Sayed, 1967; Mandelli, 1965), though new field measurements have been carried out in the past few years (Garcia et al., 2008; Lutz et al., 2010; Schloss et al., 2007; Segura et al., 2013).

Remote sensing of ocean color is an ideal tool to assess primary production on a regional and global scale, since it offers good spatial and temporal coverage providing daily estimations of the phytoplankton biomass (as indexed by chlorophyll-*a* concentration), attenuation coefficient, and photosynthetically available radiation (PAR). The ecological importance of these information remains, however, limited by the algorithms accuracy and the fact that only the upper layer (first optical depth) of the ocean is accessible to satellite-based sensors. Moreover,

Table 1
Symbols used and their units.

Symbol	Description	Units
a_d	Absorption coefficient of detritus	m^{-1}
a_{ph}	Absorption coefficient of phytoplankton	m^{-1}
a_t	Total absorption coefficient	m^{-1}
$\overline{a_{ph}}$	Spectrally averaged absorption coefficient of phytoplankton	m^{-1}
$\overline{a_{ph}^B}$	Spectrally averaged absorption coefficient of phytoplankton normalized by $Chla$	$m^2 \, (mg \, Chla)^{-1}$
b_{bp}	Particle backscattering coefficient	m^{-1}
C_{ph}	Phytoplankton carbon biomass	$mg \, m^{-3}$
$Chla$	chlorophyll-a concentration	$mg \, m^{-3}$
DL	Daylength	h
I	Irradiance	$mol \, quanta \, m^{-2} \, s^{-1}$
I_0	Daily average surface irradiance in the photosynthetically active radiation range (PAR, 400–700 nm)	$mol \, quanta \, m^{-2} \, s^{-1}$
I^n_0	Surface PAR irradiance at noon	$mol \, quanta \, m^{-2} \, s^{-1}$
K_d	Diffuse attenuation coefficient for downwelling irradiance	m^{-1}
K_ϕ	Irradiance for $\phi = \phi_m/2$	$mol \, quanta \, m^{-2} \, d^{-1}$
P_{ZT}	Daily water column primary production	$mg \, C \, m^{-2} \, d^{-1}$
P^B_m	Maximum production at saturating irradiance normalized by $Chla$	$mg \, C \, (mg \, Chla)^{-1} \, h^{-1}$
P^B_{opt}	Optimum maximum observed chlorophyll specific carbon fixation rate	$mg \, C \, (mg \, Chla)^{-1} \, h^{-1}$
SST	Sea Surface Temperature	°C
T	Time	h
Z	Depth	m
Z_m	Mixed layer depth	m
Z_{pd}	Penetration depth	m
Z_{eu}	Euphotic depth (1% I_0)	m
α^B	Initial slope of production versus irradiance normalized by $Chla$	$mg \, C \, (mg \, Chla)^{-1} \, h^{-1} \, (W \, m^{-2})^{-1}$
μ	Growth rate	divisions d^{-1}
ϕ	Quantum yield of photosynthesis	$mol \, C \, (mol \, quanta)^{-1}$
ϕ_m	Maximum quantum yield of photosynthesis	$mol \, C \, (mol \, quanta)^{-1}$
λ	Wavelength	nm

some algorithms require other information not accessible by remote sensing, such as the photosynthetic response to available light and biomass profile parameters (Platt & Sathyendranath, 1988; Sathyendranath & Platt, 1993).

In order to improve the estimation of primary production at large scale in this ecologically relevant region, the use of a combined approach using satellite and in situ observations is preferred. Algorithms in use today range from very simple and purely empirical, such as a simple relationship between $Chla$ and primary production, to highly complex models based on plant physiology, in which many variables are resolved with depth and with the spectral light (some are listed in Behrenfeld & Falkowski, 1997b; Carr et al., 2006). Some of the information required to run these models are available through remote sensing, such as sea-surface temperature (SST), PAR, and surface $Chla$ concentration; others such as the depth-resolved biomass distribution and the physiological parameters have to be extrapolated in space and time from in situ observations. Different methods of assigning relevant parameters have also been proposed (Behrenfeld & Falkowski, 1997a; Forget, Sathyendranath, Platt, Pommier, & Fuentes-Yaco, 2007; Platt et al., 2008). With the aim of estimating primary production using satellite information we first evaluated five relatively simple (non-spectral and uniform biomass profile) models to determine the most appropriate local model using field data as input. Primary production was then computed using satellite-derived products corresponding to the sampled dates (match-ups) and errors in the satellite-derived variables required by the models were evaluated. Monthly maps of primary production corresponding to the three cruises calculated from remotely sensed data and average photosynthetic parameters from each cruise provide the first synoptic views of primary production in the Argentine continental shelf and shelf-break regions.

2. Materials and methods

2.1. Primary production models

Among the wide variety of existing models for estimating ocean productivity from ocean color, three types can be identified depending on the

main variable used in the computation of primary production, i.e. chlorophyll concentration, phytoplankton carbon concentration and phytoplankton absorption. Simple versions of each model, i.e. which consider no spectral dependence and uniform biomass profile, are analyzed in the present study.

2.1.1. Chlorophyll-based models (Eppley, VGPM, BIOM)

Most of the existing models are chlorophyll-based models, but only three of them have been selected for the analysis. One of the models is a basic empirical relationship between biomass, indexed as $Chla$ concentration, and daily water-column primary production (P_{ZT}) found in Eppley, Steward, Abbott, and Heyman (1985); it ignores any external forcing or changes in physiological state of the cells and can be estimated using the following equation:

$$\log_{10} P_{ZT} = 0.5 \times \log_{10} Chla + 3.0. \tag{1}$$

The second model tested is the widely used Vertically Generalized Productivity Model (VGPM) algorithm developed by Behrenfeld and Falkowski (1997a), a model of relatively low complexity, driven by SST, daily average PAR irradiance at surface (I_0), day length (DL), $Chla$, euphotic depth (Z_{eu}), and the optimum or maximum observed chlorophyll specific carbon fixation rate within the water column (P^B_{opt}). P_{ZT} is calculated using

$$P_{ZT} = 0.66125 \times Chla \times P^B_{opt} \times DL \times \left[\frac{I_0}{I_0 + 4.1}\right] \times Z_{eu}. \tag{2}$$

The last two terms on the right side of the equation, also called the volume function, allows primary production calculated at the surface to be related to the primary production integrated in the water column. The VGPM uses a seventh order empirical temperature-dependent model to estimate P^B_{opt} as described in Eq. (11) of Behrenfeld and Falkowski, (1997a).

Finally, the third chlorophyll-based model tested was the model developed by Platt and Sathyendranath (1988) at the Bedford Institute of

Oceanography (hereafter denominated BIOM). The primary production at depth z and time t is calculated using

$$P(z,t) = Chla \times P_m^B \times \left(1 - e^{\left[-\left(\alpha^B \times I(z,t)/P_m^B\right)\right]}\right). \tag{3}$$

where α^B is the initial slope of the photosynthesis–irradiance (P–I) curve (at light-limited conditions), P_m^B is the assimilation number (the plateau reached under light-saturating conditions of irradiance I), and $I(z,t)$ is PAR irradiance at depth z and time t, and can be expressed as an exponential decay of surface PAR (I_0) at time t.

$$I(z,t) = I_0(t) \times e^{\left(-K_d(\text{PAR}) \times z\right)} \tag{4}$$

where K_d(PAR) is the downwelling diffuse attenuation coefficient of PAR irradiance. For the time dependence, the surface irradiance I_0 is assumed to follow a sinusoid $I_0(t) = I^n_0 \sin(\pi/DL)$, where the light day runs from sunrise ($t=0$) to sunset ($t=DL$), and I^n_0 is the surface irradiance at local noon. The daily water column integrated primary production, P_{ZT}, is then calculated integrating Eq. (3) in the whole column and throughout the day length, which is calculated taking into account the latitude and day of the year. The largest assumption underscoring Eq. (3) is that P_m^B and α^B are constant as a function of depth and time.

2.1.2. Carbon-based model (CbPM)

The carbon-based productivity model (CbPM), developed by Behrenfeld, Boss, Siegel, and Shea (2005), abandons the traditional chlorophyll-based approach and instead of relating P_{ZT} to Chla and physiological parameters, like P^B_{opt}, it relates P_{ZT} to phytoplankton carbon biomass (C_{ph}) and growth rate (μ) and is estimated using

$$P_{ZT} = C_{ph} \times \mu \times \left[\frac{I_0}{I_0 + 4.1}\right] \times Z_{eu}. \tag{5}$$

As in Eq. (2), the last two terms are the same volume function used in the VGPM model which relates surface to water column primary production. The C_{ph} (mg m^{-3}) is estimated from the particle backscattering coefficient at 443 nm ($b_{bp}(443)$) ($C_{ph} = 13{,}000 \times (b_{bp}(443) - 0.00035)$), and μ (cell divisions d^{-1}) is estimated from chlorophyll-to-carbon ratio ($Chla$:C_{ph}). Phytoplankton growth rate is calculated from the maximum potential growth rate of a natural assemblage (set to 2 divisions per day based on Banse, 1991) and corrected for the suppression of growth rate by nutrient and temperature stress and light limitation (see Behrenfeld et al., 2005 for details). This model requires the attenuation coefficient at 490 nm ($K_d(490)$) and the backscattering coefficient at 443 nm, $b_{bp}(443)$. Since these data were not estimated in the field, they were taken from MODIS-Aqua derived products $K_d(490)$ and $b_{bp}(443)$ composite maps for each cruise period at each sample location (i.e., this model could not be tested using only field data, but a combination of field and satellite derived information).

2.1.3. Absorption-based model (AbPM)

A simplified (spectrally integrated) absorption-based model based on Lee, Carder, Marra, Steward, and Perry (1996) and Marra, Trees, and O'Reilly (2007) was tested. The algorithm (hereafter denominated AbPM) is based on irradiance (I), the spectrally averaged absorption of irradiance by phytoplankton ($\overline{a_{ph}}$), and the quantum efficiency (ϕ) with which that irradiance is converted to fixed carbon

$$P(z) = \phi(z) \times \overline{a_{ph}} \times I(z). \tag{6}$$

The quantum yield (ϕ) can be influenced by irradiance (Kiefer & Mitchell, 1983) which dependence can be described by

$$\phi(z) = \phi_m \times \frac{K_\phi}{K_\phi + I(z)} \tag{7}$$

where ϕ_m is the maximum quantum yield and K_ϕ is the irradiance at which ϕ reaches half its maximum value. In the present study, values of ϕ_m were taken from field measurements ($\alpha / \overline{a_{ph}}$) and $K_\phi = 10$ mol quanta m^{-2} d^{-1} was used as suggested by Kiefer and Mitchell (1983). The irradiance at depth, $I(z)$, is calculated as in Eq. (4) by an exponential decay of the surface irradiance I_0. Thus re-writing Eq. (6) using Eqs. (7) and (4), the primary production at depth z is calculated using

$$P(z) = \phi_m \times \frac{K_\phi}{K_\phi + I_0 \times e^{(-K_d(\text{PAR}) \times z)}} \times \overline{a_{ph}} \times I_0 \times e^{(-K_d(\text{PAR}) \times z)}. \tag{8}$$

Then P_{ZT} is obtained integrating Eq. (8) in the whole water column. It should be noted that no photoinhibition factor was applied, as in Lee et al. (1996), given that field data for the cruises analyzed did not show photoinhibition except at one station.

2.2. Field data

Three extensive campaigns on board R/V *ARA Puerto Deseado* were performed during spring (GEF-1: October 2005), late summer (GEF-2: March 2006) and late winter (GEF-3: September 2006) over the Argentine continental shelf (38°–55°S) (Fig. 1). Fixed stations were sampled and continuous profiles of temperature and salinity were determined using a Sea-Bird 911 CTD. At these stations (marked with crosses in Fig. 1) surface water samples were collected using a bucket, and at two or three selected depths using Niskin bottles for Chla and particulate absorption determinations. At selected stations (marked with circles in Fig. 1), surface samples were used to run P–I incubation experiments. In addition, between stations, seawater samples for analysis of Chla were taken approximately every 2 h from the flow-through system (marked with dots in Fig. 1). Table 2 shows the number of sampled stations where CTD profiles were performed and particulate absorption was measured (St–Abs), stations where P–I experiments were run (St–P) and the total number of stations where Chla was determined (St–Chla) per cruise.

Chlorophyll-a concentration was determined using the fluorometric method of Holm-Hansen, Lorenzen, Holmes, and Strickland (1965) modified by Lutz et al. (2010), photosynthetically active radiation (PAR, 400–700 nm) irradiance at the surface was recorded continuously during the cruises with a cosine downwelling irradiance (LI-COR) sensor, and PAR downwelling diffuse attenuation coefficient (K_d(PAR)), was modeled following the parameterization proposed by Sathyendranath and Platt (1988). Total and detritus absorption spectra ($a_t(\lambda)$ and $a_d(\lambda)$, respectively) were obtained following the quantitative method of Mitchell (1990) using the pathlength amplification factor given by Hoepffner and Sathyendranath (1992). The phytoplankton absorption coefficient, $a_{ph}(\lambda)$, was calculated by subtracting $a_d(\lambda)$ from $a_t(\lambda)$. Then, the specific absorption coefficient of phytoplankton, $\overline{a_{ph}^B}$, was calculated normalizing by Chla and averaging over the spectral range between 400 and 750 nm. P–I incubation experiments were run using the ^{13}C method of Hama et al. (1983). Surface water samples were incubated for 3 h in a light-gradient incubation box maintaining the temperature close to that of the sea. The initial slope (α^B) and the biomass-normalized photosynthetic rate at saturating irradiance (P^B_m) were estimated from the P–I experiments by fitting the exponential equation of Platt, Gallegos, and Harrison (1980) to the data. The same equation was used to estimate the daily integrated primary production (P_{ZT}) using the photosynthetic parameters obtained from the surface water sample incubations and the Chla concentration profile, and integrating it throughout the daylength and the whole water column. A detailed account of the experimental procedure is given by Lutz et al. (2010).

The euphotic depth (Z_{eu}) is here defined as that where the PAR is reduced to 1% of its surface value and the mixed layer depth (Z_m) as the depth at which the potential density in the upper layer changes by 0.05 kg m^{-3} relative to the ocean surface density. This criterion was selected based on the results obtained by Reta (2009) who examined the
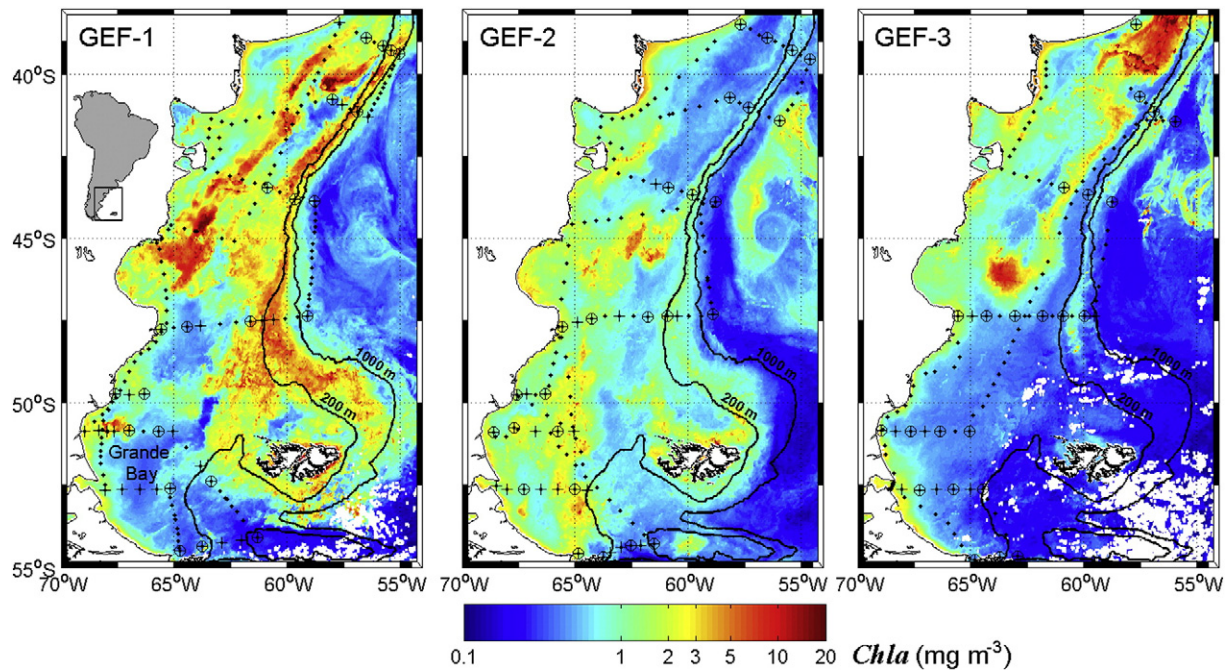
Fig. 1. Composite images of *Chla* (mg m^{-3}) derived from MODIS-Aqua (OC3Mv6) spanning the time period from October 8–28, 2005 (GEF-1), March 10–April 1, 2006 (GEF-2), and September 5–25, 2006 (GEF-3). Symbols indicate collection of samples for: *Chla* (dots), particulate absorption (crosses), and *P–I* experiments (circles).

distribution of physical properties within the upper layer using all the CTD profiles of the three campaigns and compared different criteria and thresholds for determining the depth of the mixed layer depth. In order to analyze the stability of the water column, the Simpson parameter was calculated as in Bianchi et al. (2005) and the ratio between the euphotic and the mixed layer depths (Z_{eu}:Z_m) was computed as an index of the vertical light availability (i.e., if this ratio < 1, phytoplankton would be mixed below the euphotic zone; if >1, it will remain always in the illuminated zone). The former takes into account only the physical characteristics and the latter the physical and biological characteristics of the water column. Then, stations were classified according to the critical values for each index; for the Simpson parameter the value of 50 J m^{-3} was used to determine whether the water column was well-stratified ($\geq$50 J m^{-3}) or homogeneous (<50 J m^{-3}). This value was used in Bianchi et al. (2005) to estimate the mean frontal position in summer using a large hydrographic database available in this region. Alternatively, Z_{eu}:Z_m ratios higher and lower than 1 indicated well-illuminated or potentially light-deprived conditions, respectively. Finally, we estimated the penetration depth (Z_{pd}), i.e. the depth from which information can be collected by sensors on board of spacecrafts, as Z_{eu}/4.6, an approximation which corresponds to about the first quarter (22%) of the euphotic zone.

2.3. Satellite data

MODIS-Aqua daily Level 1A and ancillary data corresponding to the dates of the cruises were downloaded from the NASA Ocean Color website (http://oceancolor.gsfc.nasa.gov). Full resolution (1.1 km) Local

Table 2
Summary of the research cruises conducted in the Argentine shelf and shelf-break on board the R/V *ARA Puerto Deseado* where particulate absorption measurements (St–Abs), primary production experiments (St–P) and *Chla* estimations (St–*Chla*) were performed.

Cruise	Period	Season	St–Abs	St–P	St–*Chla*
GEF-1	8–28 October 2005	Spring	41	22	166
GEF-2	10 March–1 April 2006	Summer	40	25	142
GEF-3	5–25 September 2006	Winter	30	23	121
All			**111**	**70**	**429**

Area Coverage (LAC) images were processed using SeaDAS v6.2 (2009 reprocessing) and the following products were obtained: *Chla*, using OC3Mv6 algorithm; PAR product (http://oceancolor.gsfc.nasa.gov/DOCS/seawifs_par_wfigs.pdf); K_d(PAR) using the model of Lee et al. (2007) for estimating the euphotic depth; b_{bp} at 443 nm as derived using the GSM model (Maritorena, Siegel, & Peterson, 2002); and *SST* daytime product (11 μm band). For the L1A to L2 processing, pixels with excessive cloud cover, large solar and sensor zenith angles (>70° and >60°, respectively), and sun glint contamination or where sensors saturate, were masked out.

For the evaluation of satellite estimates (match-up analysis), the median value of each product in a 3×3 pixel box centered at the location of the sample sites and with ± 12 h time difference between the satellite overpass and the sampling was extracted and used to compare with field measurements. Quality of the satellite retrieval was assessed using the standard masks and flags (Bailey & Werdell, 2006), a minimum number of pixels (5 out of 9) should be valid and the standard deviation should be below 20% of the mean to consider it a valid match-up.

Satellite-derived and modeled values were regressed against field data and a type II linear regression model was applied since both field and modeled data are subject to error. The slope, intercept and the correlation coefficient (r) were determined. In the case of *Chla*, the regression was performed between log-transformed values. To assess the overall models and algorithm performance, the relative percent *bias* (a measure of accuracy), the mean relative Absolute Percent Difference, APD (a measure of average relative uncertainty), and the root mean square error, RMSE (a measure of the average magnitude of the error), were computed. These errors are defined as follow:

$$\text{Bias} = \frac{1}{n}\sum \left(\frac{X^m - X^f}{X^f} \right) \times 100, \tag{9}$$

$$\text{APD} = \frac{1}{n}\sum \left(\frac{\left| X^m - X^f \right|}{X^f} \right) \times 100, \tag{10}$$

$$\text{RMSE} = \sqrt{\frac{1}{n}\sum \left(X^m - X^f \right)^2}, \tag{11}$$

where X^m and X^f are the modeled and field variables analyzed, respectively, and n is the number of observations.

3. Results

3.1. Field data: Primary production, photosynthetic parameters and other variables

The daily integrated water-column primary production for the three cruises ranged from 52.5 mg C m^{-2} d^{-1} at a southern station during the summer cruise (54°20.79′S, 62°31.78′W, GEF-2), to 5477.5 mg C m^{-2} d^{-1} at a station located in the north at the shelf-break during the spring cruise (39°15.42′S, 55°23.04′W, GEF-1). Higher and a wider range of values were observed during GEF-1 (spring) compared to GEF-2 and GEF-3 cruises (late summer and late winter, respectively) (Table 3). Discrete and sparse field P_{ZT} estimations (with limited spatial resolution) performed in large areas characterized by the presence of phytoplankton blooms, such as the Argentinean shelf, might not always represent well its spatial variability. In particular, GEF-3 cruise was performed during late winter and two different conditions were found in the northern and southern part of the study area. Lower values, more representative of winter season, were generally found south of ~47°S (minimum value of 71.7 mg C m^{-2} d^{-1}), while higher values were found to the north, indicating already the beginning of spring (maximum value of 629.0 mg C m^{-2} d^{-1}). Therefore, even though similar ranges of P_{ZT} were found in summer and winter cruises, during the latter lower values were more frequently found (70% of the measurements were performed south of 47°S) than during late summer cruise (median values of 122.4 mg C m^{-2} d^{-1} and 279.7 mg C m^{-2} d^{-1}, for GEF-3 and 2 respectively).

The photosynthetic parameters (α^B and P^B_m) showed a similar behavior. They were highly variable in the three cruises, higher values were found in spring (maximum values of 0.84 mg C (mg $Chla$)$^{-1}$ h^{-1} (W m^{-2})$^{-1}$ and 10.05 mg C (mg $Chla$)$^{-1}$ h^{-1}, respectively) and lower in late summer and late winter cruises (Table 3). Variability was higher in the summer cruise (CV = 40% and 68% for α^B and P^B_m, respectively) than in the winter cruise (CV = 24% and 28% for α^B and P^B_m, respectively).

Surface $Chla$ distribution was better described given the more intense sampling (N = 429) compared to P_{ZT} estimations (N = 70). Satellite-derived $Chla$ distributions (Fig. 2) resembled the main features depicted by in situ measurements (see details in Segura et al., 2013). During the spring cruise strong blooms were found associated to several oceanic and coastal frontal systems with a maximum value of chlorophyll concentration of 24.01 mg m^{-3} in Grande Bay (no P_{ZT} data). Blooms with reduced intensity during the late summer cruise were found, while during the late winter cruise low $Chla$ values were found south of ~47°S (minimum value of 0.45 mg m^{-3}) and relatively high values (maximum of 7.95 mg m^{-3}) were found to the north indicating the beginning of spring in this region (see Fig. 2 in Segura et al., 2013). In the same fashion as the photosynthetic parameters, K_d(PAR) also showed similar ranges for the summer and winter cruises and slightly higher values and variability for the spring cruise (CV = 10%, 12% and 50% for summer, winter and spring cruises, respectively). In contrast, a^B_{ph}

values were higher and more variable in late summer cruise (GEF-2) compared to the other cruises.

3.2. Models' performance using field data

The five models previously described were tested using field data as input when available and compared to field estimates of P_{ZT}. Strictly speaking, the analysis performed regarding the BIOM model assesses its performance when vertically homogeneous biomass profile is considered, since the same basic equation is used to estimate field P_{ZT}. Another caveat to consider is that all the input values required for Eppley and BIOM models were available, while for VGPM, CbPM and AbPM some of the variables were modeled, taken from literature or from remotely sensed data, i.e. P^B_{opt} was modeled from field SST for VGPM, $b_{bp}(443)$ and $K_d(490)$ were taken from MODIS-Aqua composites for each cruise period for CbPM, and K_ϕ for AbPM was taken from the literature (Kiefer & Mitchell, 1983).

Fig. 2 displays the scatter plots of the modeled versus field P_{ZT} values for the chlorophyll − (Eppley, VGPM and BIOM), carbon- and absorption-based models. The statistical performances of all the models are presented in Table 4. The reduced number in the values retrieved using the CbPM ($n = 66$) compared to the other models ($n = 70$) is caused by missing values of satellite-derived products (required to estimate backscattering not measured in the field) due to the presence of clouds (especially in the south in winter) and stations located too close to land which are also masked due to straylight contamination. A significant correlation was found between modeled and field P_{ZT} values for all the models analyzed, except for the CbPM. However, a high degree of scatter in the data is apparent for all the models, except for BIOM (Fig. 2). This model, not surprisingly, gave the closest results compared to the field ones since both were computed with similar equations; it showed a high correlation ($r = 0.99$, $p < 0.00001$), the lowest mean error (RMSE = 112.3 mg C m^{-2} d^{-1}) and a small negative $bias$ (−3.06%). The AbPM showed a high correlation ($r = 0.90$, $p < 0.00001$), but a slope close to 0 (0.13), showing a systematic underestimation ($bias = -82.9\%$) and a high mean error (RMSE = 876.6 mg C m^{-2} d^{-1}). The VGPM and Eppley models showed the least accurate estimations with high overestimation (192.8 and 367.6% $bias$, respectively), high RMSE (786.8 and 870.4 mg C m^{-2} d^{-1}, respectively), and large APD (204.0 and 374.0%).

Considering the seasons separately, most of the models, except BIOM and AbPM, overestimated field values in summer (GEF-2) and winter (GEF-3) cruises (grey and white symbols in Fig. 2). On the other hand, high dispersion of the points around the 1:1 line was observed for the spring data set (GEF-1 cruise, black symbols). Analyzing the statistics by season, all of the models showed a significant correlation, except CbPM in spring and summer (Table 5). In general, higher correlations were found in winter and lowest in summer, which also showed the highest relative errors and $bias$. Although greater confidence and lower $bias$ and APD were obtained in spring retrievals compared to the summer, larger mean average errors (RMSE) were still present, mainly due to higher absolute errors associated with increased values of P_{ZT} in spring. Finally, most of the models explained a high

Table 3
Range, mean and median values of the variables used as inputs to the primary production models for each cruise. See Table 1 for definitions and units.

Variables	GEF-1		GEF-2		GEF-3	
	Range	Mean (median)	Range	Mean (median)	Range	Mean (median)
P_{ZT}	275.1–5477.5	1271.9 (759.6)	52.5–625.3	298.2 (279.7)	71.7–629.0	183.4 (122.4)
P^B_m	0.73–10.05	4.07	0.71–6.14	2.20	0.68–1.97	1.04
α^B	0.04–0.84	0.26	0.03–0.10	0.07	0.03–0.08	0.05
ϕ_m	0.002–0.042	0.013	0.001–0.005	0.003	0.004–0.002	0.003
$Chla$	0.57–19.1	2.93 (1.19)	0.65–4.24	1.36 (1.1)	0.42–4.38	1.25 (0.9)
K_d(PAR)	0.16–0.39	0.20	0.16–0.23	0.19	0.17–0.26	0.18
a^B_{ph}	0.006–0.022	0.011	0.007–0.024	0.017	0.006–0.018	0.011
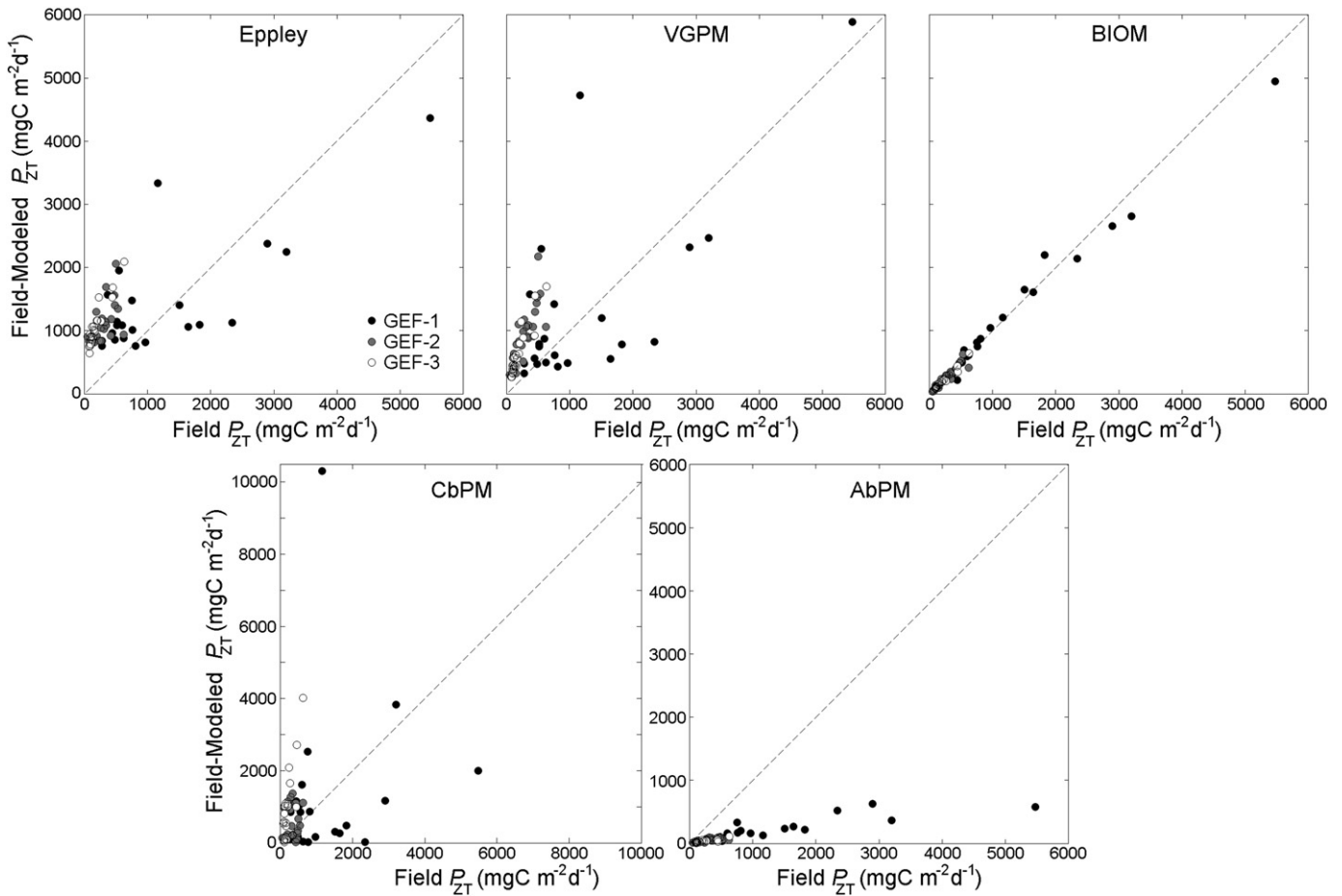
Fig. 2. Modeled P_{ZT} using as input field measurements and/or mean satellite-derived values versus field estimates, for the chlorophyll-based models: Eppley, VGPM and BIOM (upper row) and the carbon- and absorption-based models: CbPM and AbPM (lower row). Cruises are indicated with black (GEF-1, spring), grey (GEF-2, summer), and white (GEF-3, winter) symbols.

percentage of the variability for the winter data ($r > 0.85$), being in general more precise and accurate (lower APD and *bias*) than when applied to the summer data (except for the Eppley model), but less accurate than the spring cruise, showing higher overestimations (*bias*) and uncertainties (APD).

3.3. Primary production using satellite data

Given that BIOM provided the best estimates, further analysis using satellite-derived values was carried out using this model. In order to understand how the estimates of P_{ZT} can be affected by errors in the satellite-derived data, a match-up analysis was performed between field measurements and satellite-derived products used in this model. Then, the modeled P_{ZT} using satellite data as input acquired concomitant with in situ measurements were compared to field estimations.

3.3.1. Validation of satellite-derived products

A total of 104, 33 and 36 match-ups were obtained for *Chla*, K_d(PAR) and PAR products, respectively. Scatter plots are shown in Fig. 3 and coefficients and statistics of the regressions are presented in Table 6.

An overall good correlation between field and satellite-derived products was observed with correlation coefficients ranging from 0.68 to 0.83 (Table 6). On average, *Chla* is underestimated by MODIS-Aqua OC3v6 algorithm by −28.6%, has a RMSE of 1.98 mg m^{-3}, and a relative large APD

Table 4
Statistical results for the modeled P_{ZT} using Eppley, VGPM, BIOM, CbPM and AbPM models: APD (%), RMSE (mg C m^{-2} d^{-1}) and *bias* (%). Slope, intercept of a type-II linear regression model, correlation coefficient (r) and the number of data points (n) are also given.

Model	Slope	Intercept	r	RMSE	*bias*	APD	n
Eppley	0.61	862.82	0.72	870.4	367.6	374.0	70
VGPM	1.10	354.50	0.71	786.8	192.8	204.0	70
BIOM	0.93	20.54	0.99	112.3	−3.06	10.1	70
CbPM	4.48	−1710.71	0.24*	1516.4	182.3	228.4	66
AbPM	0.13	15.49	0.90	876.6	−82.9	82.9	70

* Not significant.

Table 5
Statistical results for the modeled P_{ZT} using Eppley, VGPM, BIOM, CbPM and AbPM models as a function of season for each model: APD (%), RMSE (mg C m^{-2} d^{-1}) and *bias* (%). Slope, intercept of a type-II linear regression model, correlation coefficient (r) and the number of data points (n) are also given.

Model	Season	Slope	Intercept	r	RMSE	*bias*	APD	n
Eppley	Spring	0.65	633.44	0.75	838.9	72.8	93.2	22
	Summer	2.89	261.17	0.61	862.6	403.8	403.8	25
	Winter	2.52	604.30	0.95	907.5	610.2	610.2	23
VGPM	Spring	1.21	−163.52	0.69	1046.1	41.8	77.5	22
	Summer	3.34	−41.38	0.79	729.9	260.1	260.1	25
	Winter	2.90	90.27	0.93	508.2	264.0	264.0	23
BIOM	Spring	0.91	80.64	0.99	189.2	−1.4	9.5	22
	Summer	0.99	−7.54	0.94	56.1	−4.3	13.6	25
	Winter	0.95	−0.31	0.98	27.2	−3.4	6.8	23
CbPM	Spring	7.41	−8114.82	0.16*	2309.4	45.6	131.7	22
	Summer	−53.22	17013.6	−0.05*	569.7	180.6	207.7	24
	Winter	8.07	−642.06	0.86	1154.1	334.7	359.5	20
AbPM	Spring	0.12	47.92	0.85	1521.4	−83.0	83.0	22
	Summer	0.14	10.37	0.74	280.3	−81.6	81.6	25
	Winter	0.13	3.37	0.86	197.6	−84.2	84.2	23

* Not significant.
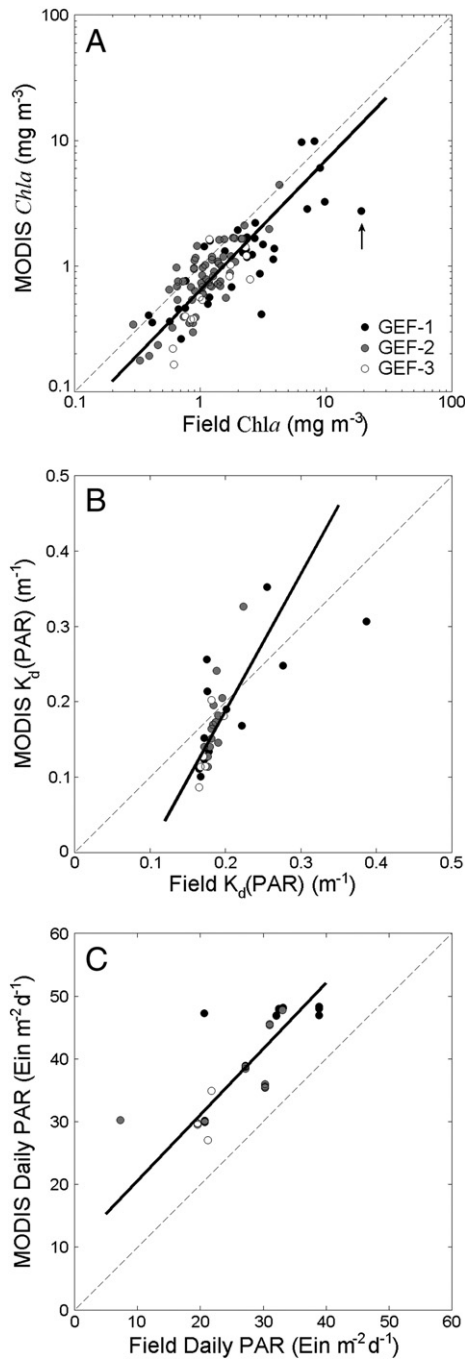
Fig. 3. MODIS-derived versus field estimations of A) *Chla*, B) K_d(PAR), and C) daily PAR irradiance products. The arrow indicates a match-up pair that was highly underestimated by the satellite-derived products. Cruises are indicated with black (GEF-1), grey (GEF-2), and white (GEF-3) symbols. The dashed line represents the 1:1 relationship.

(36.9%). K_d(PAR) product (Lee et al., 2007) also tends to underestimate field values (*bias* = −9.8%) and have high APD (22.1%) and a RMSE of 0.05 m^{-1}. In contrast, PAR product tends to overestimate field values by ~50%, with an APD of 48.8% and a RMSE of 12.28 mol quanta m^{-2} d^{-1}.

3.3.2. Comparison between field and satellite-derived P_{ZT}

A total of 19 match-up pairs were obtained with simultaneous satellite and field primary production estimates (Fig. 4). In this case all the inputs of the model were satellite-derived products, except for the photosynthetic parameters (α^B and P^B_m) that were estimated from field P–I experiments. A relative high correlation ($r = 0.70$, $p < 0.001$), but high RMSE (1041.5 mg C m^{-2} d^{-1}) and a slope closer to 0 than to

Table 6
Statistical results for the MODIS-derived products used as input to the models and P_{ZT} using satellite-derived products: APD (%), RMSE (same units as the variable, see Table 1) and *bias* (%). Slope, intercept of a type-II linear regression model, correlation coefficient (r) and the number of data points (n) are also given.

	Slope	Intercept	*r*	RMSE	*bias*	APD	*n*
Chla	1.04	−0.19	0.81	1.98	−28.6	36.9	104
K_d(PAR)	1.82	−0.18	0.68	0.05	−9.8	22.1	33
PAR	1.05	10.00	0.83	12.28	48.8	48.8	36
P_{ZT}	0.95	−13.12	0.93	85.8	−7.0	22.2	18

1 (0.15) was found (not shown). This is clearly caused by a station for which P_{ZT} was highly underestimated (shown by the arrow in Fig. 4A). This station, located in the north of the shelf break and sampled during GEF-1 spring cruise, showed a high *Chla* (19.05 mg m^{-3}) and the highest P_{ZT} values of all the three cruises (5477.5 mg C m^{-2} d^{-1}). *Chla* at this station was highly underestimated by the MODIS-Aqua product (see arrow in Fig. 4A) thus influencing the modeled P_{ZT}. When this station is not included in the analysis, a better performance of the model is obtained (Fig. 4B) with a correlation of 0.93 ($p < 0.00001$), a slope close to 1 (0.95), and small RMSE (85.8 mg C m^{-2} d^{-1}). However, a relatively small negative *bias* (−7.0%) and APD of 22.2% is still observed (Table 6).

4. Discussion

The highest values of P_{ZT} were found during the spring cruise (GEF-1) associated with the dominance of *Thalassiosira* cf *oceanica* (Sabatini et al., 2012) in the shelf-break region, and with the predominance and blooming state of the dinoflagellate *Prorocentrum minimum* (Gómez et al., 2011; Sabatini et al., 2012; Segura et al., 2013) in Grande Bay (Fig. 1). The range of values for P_{ZT} in the continental shelf region was higher than reported by El-Sayed (1967) for a comparable season (100–1500 mg C m^{-2} d^{-1}). At the shelf-break, P_{ZT} ranged between 440 and 5470 mg C m^{-2} d^{-1}, values higher than those reported by Negri (1993) in a region close to the shelf-break at 39°S during April–December (100–2700 mg C m^{-2} d^{-1}). Similarly, Garcia et al. (2008) found higher values of P_{ZT} (1960–7790 mg C m^{-2} d^{-1}) in the shelf-break region in spring 2004 (November) for stations also numerically dominated by species of the genus *Thalasiossira*; this could be related to a different stage of the bloom and thus different physiological state of the phytoplankton community (Forget et al., 2007). Differences could also be partly related to the different methods used for estimating P_{ZT}.

P_{ZT} values found during the late summer cruise (GEF-2) were lower than during the spring cruise (GEF-1), and lower than the values found by El-Sayed (1967) during a late summer cruise in February–March 1963 (400–1400 mg C m^{-2} d^{-1}). During the winter cruise (GEF-3) P_{ZT} values were generally low (mean value of 183.4 mg C m^{-2} d^{-1}) and lower than those reported by El-Sayed (1967) in August–October 1963, ranging from 0 to 1000 mg C m^{-2} d^{-1} with a mean value of 500 mg C m^{-2} d^{-1}. This can be due, at least in part, to differences in the methods used and most probably to the natural inter-annual variability already found by El-Sayed (1967). In spite of these differences in magnitude between the values found in the present study and those obtained in the extensive study performed by El-Sayed in the 1960s, both works report high P_{ZT} values during spring, lower in summer and the lowest in late winter.

4.1. Models' performance using field data

Chlorophyll-based models have been widely used since chlorophyll-*a* plays a central role in the process of photosynthesis, is ubiquitous in all photosynthetic organisms (or replaced by close chemical forms such as bacterio-chlorophyll-*a* or divinyl-chlorophyll-*a*), and variation in the amount of *Chla* can account for much of the variation in observed primary production. Variability in surface *Chla* found in the shelf and
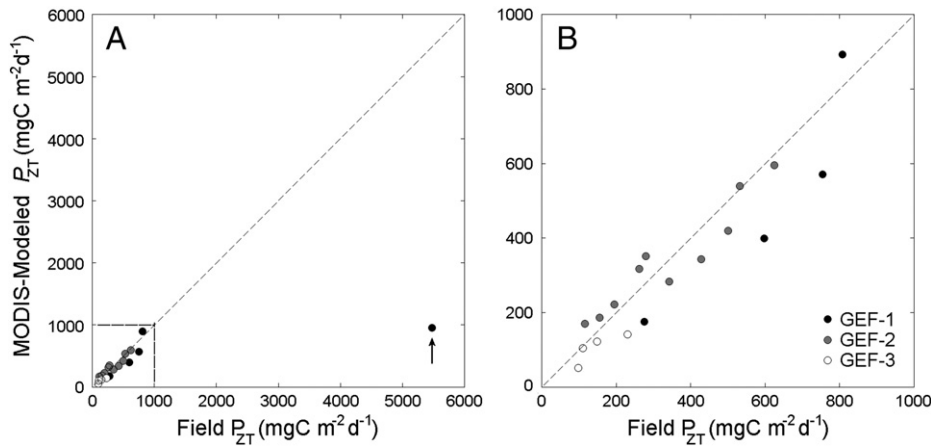
Fig. 4. A) Modeled P_{ZT} using BIOM with satellite-derived values and field photosynthetic parameters versus field estimations ($n = 19$). The arrow indicates an outlier (see text for details), B) match-up pairs that remained when the outlier has been excluded in the analysis ($n = 18$). Cruises are indicated with black (GEF-1), grey (GEF-2), and white (GEF-3) symbols. The dashed line represents the 1:1 relationship.

shelf-break regions for all the cruises analyzed explained ~56% of the variability for integrated production (not shown). Therefore, although *Chla* is generally considered as a good proxy for phytoplankton biomass, it offers only a rough indication of primary production in this region. The poor performance of the Eppley model, which uses a simple relation between *Chla* and P_{ZT} (Eq. 1), confirms this and suggests that the standing stock is not the sole determinant of photosynthetic rate, i.e. external forcing, or changes in community structure and its physiological state are probably influencing the photosynthetic efficiency of the phytoplankton community, all of which are ignored in this relative simple model. A similar poor performance was found for the VGPM model. This could be in part attributed to the lack of correlation between *SST* and P^B_{opt} proposed in the model. Even though P^B_{opt} and P^B_m are different parameters (i.e., obtained by different experimental means), they hold common information, and no significant correlation was found between the light-saturated photosynthesis parameter (P^B_m) and *SST* with the present data set. Moreover, the data didn't fit the seventh order polynomial function used in the model (Behrenfeld & Falkowski, 1997a) or the exponential function based on Eppley (1972) as implemented by Antoine and Morel (1996), especially for the spring cruise data (Fig. 5). Even though P^B_m values found in the summer and winter cruises tend to increase with *SST*, spring data clearly does not follow this trend. Results from a cluster analysis performed on the photosynthetic and bio-optical properties from the three cruises together distinguished 11 photosynthetical and bio-optical phytoplankton types (PBPTs) and in particular, the spring cruise showed the highest diversity of PBPTs (9 types) compared to the other cruises which showed only 5 PBPTs each (Segura et al., 2013). Thus, a more complex interaction between different phytoplankton types found in this cruise, light regimes, and probably nutrient availability could be influencing, more than *SST* alone, the photosynthetic efficiency of the phytoplankton community. This lack of temperature-dependence of light-saturated photosynthesis has been observed in other regions (Bouman, Platt, Sathyendranath, & Stuart, 2005; Son, Campbell, Dowell, Yoo, & Noh, 2005). No significant correlation was found between the photosynthetic parameters and environmental proxies that can be derived from satellite remote sensing data, like *Chla* and *SST*, for each cruise and for all the cruises together (Fig. 6).

Absorption-based models rely on the hypothesis that the absorption properties of phytoplankton are a response to environmental factors since they result from a certain phytoplankton community structure (species), their pigment composition (Claustre et al., 2005), and their state of photoacclimation. Thus, the absorption properties might govern, or at least indicate their physiological state (Cullen, 1990). As a consequence, near-surface productivity can be expressed in terms of phytoplankton absorption regardless of the temperature, nutrient, or

irradiance regime (Marra et al., 2007). The simplified absorption-based model (AbPM) assessed in this study (Eq. 8) showed a good correlation between estimated and field P_{ZT} values ($r = 0.90$, $p < 0.00001$), nevertheless a general underestimation of field data was found (slope close to 0 and mean *bias* of approximately −80%). One possible source of error could be the use of a fixed value for K_ϕ. This new variable introduced in this model, that cannot be directly measured and for which we have no independent means of estimating it, was taken from the literature and further understanding of its variability with regard to environmental drivers is needed to correctly assess its value (Marra, Ho, & Trees, 2003).

The CbPM showed the poorest performance of all the models analyzed, with no significant correlations between modeled and field P_{ZT} values, except for the winter cruise (Table 5). This model uses remote sensing retrievals of particulate backscattering coefficients to quantify particulate organic carbon, which is assumed to represent phytoplankton carbon concentration (C_{ph}), and chlorophyll-to-carbon ratios to estimate growth rate. In this work at each station satellite-derived mean values of $b_{bp}(443)$ and $K_d(PAR)$ for the duration of each cruise were used instead of simultaneous field and satellite data, which could in part explain the poor performance of the model. But, even when the
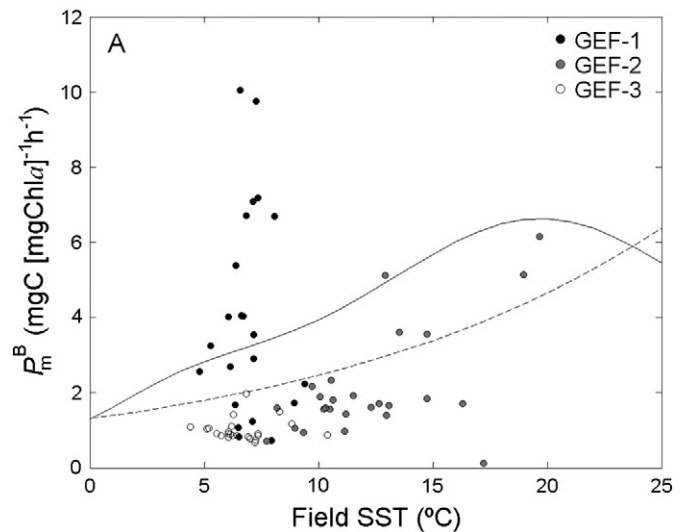
Fig. 5. The light-saturated photosynthesis parameter (P^B_m) plotted against temperature for the three cruises. The solid line is the seventh-order polynomial function of Behrenfeld and Falkowski (1997a) and the dashed line is the exponential function based on Eppley (1979) as implemented by Antoine and Morel (1996). Cruises are indicated with black (GEF-1), grey (GEF-2), and white (GEF-3) symbols.
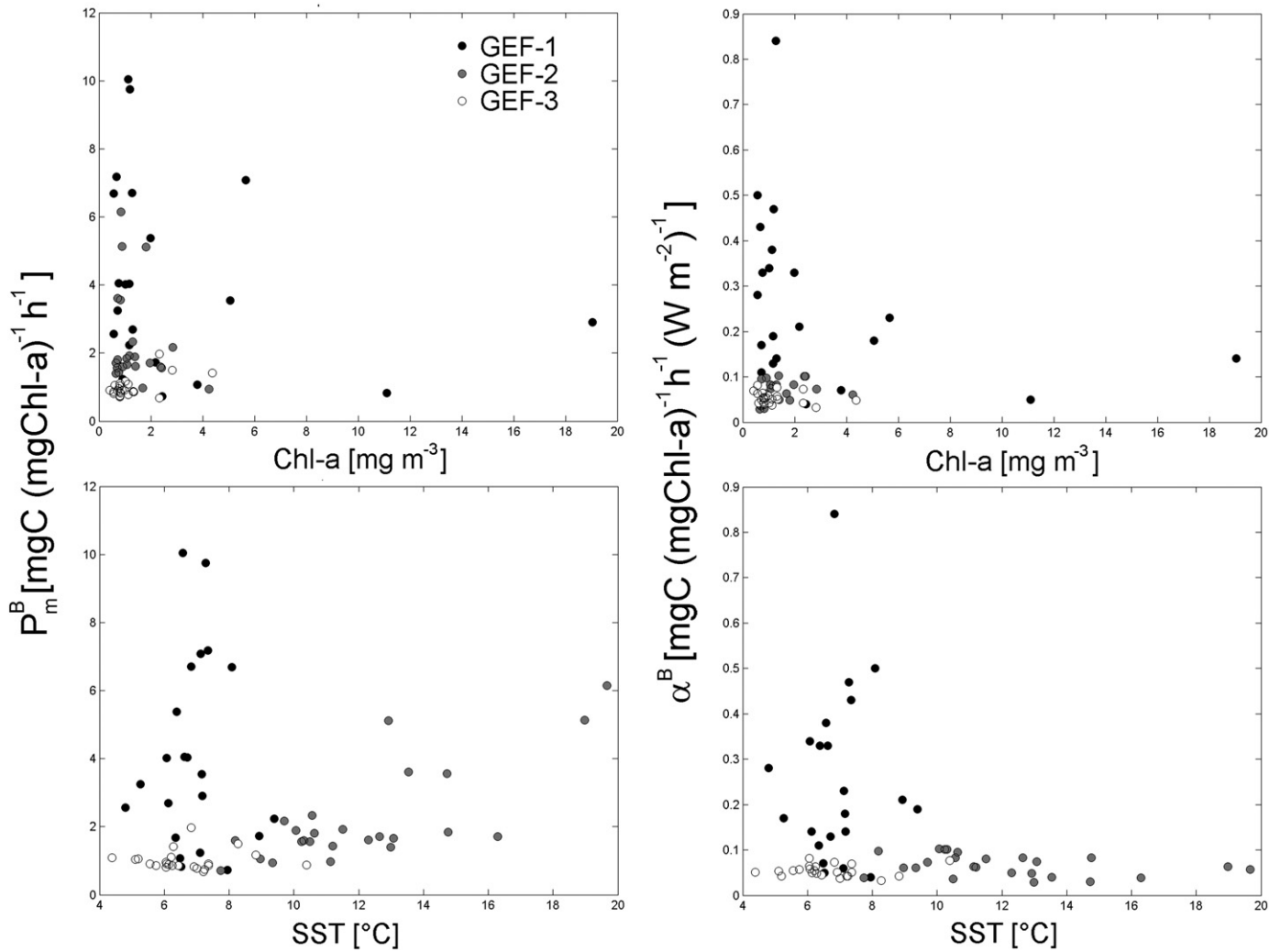
Fig. 6. Photosynthetic parameters P^B_m (left) and α^B (right) versus chlorophyll-a concentration (top row) and temperature (bottom row). Cruises are indicated with black (GEF-1), grey (GEF-2), and white (GEF-3) symbols (modified from Dogliotti, Segura, & Lutz, 2012).

model was applied only to a few match-up data pairs (i.e., not using mean values of $b_{bp}(443)$ and $K_d(PAR)$ for the whole cruise), no improvement was observed (not shown). The number of modeled values was reduced to 24 (compared to 66), the correlation was not significant (for each and all cruises together), and larger errors and uncertainties were obtained (RMSE = 2215.1 mg C m^{-2} d^{-1}, *bias* = 254.9%, and APD = 276.1%). Besides, the estimation of C_{ph}, calculated from $b_{bp}(443)$, could be biased in the coastal stations due to the presence of sediments resulting from re-suspension events. Moreover, the assessment of the MODIS $K_d(490)$ product could not be performed, which might probably add another source of error to the estimates.

BIOM showed the best performance of all the models analyzed, however small differences with field P_{ZT} estimates were still found when each cruise was considered separately (Table 5). It should be noted that the same equation (Eq. 3) was used to calculate field P_{ZT}, but in the latter, vertical variation of light and *Chla* was taken into account (more details in Lutz et al., 2010). Thus, the differences found are mainly related to the assumption of uniform biomass profiles in the simplified model assessed in this study. When considering the physical stratification, i.e. the Simpson parameter (triangles in Fig. 7), it can be observed that stations located along the shelf-break (200 m isobath) were stratified in the three cruises and stations located in the well mixed side of coastal and tidal fronts were homogeneous (open triangles in Fig. 7), while all the stations located in the mid-shelf were stratified during the summer cruise only (grey triangles in Fig. 7). However, when we consider

as an index of light availability the $Z_{eu}:Z_m$ ratio (round symbols in Fig. 7), it is clear that both indexes do not usually agree and in most of the southern shelf stations ($<47°$S) light was attenuated ($<1\%\,I_0$) before the mixed layer depth during the three cruises (open circles), while in the northern stations light penetrated deeper than the mixed layer in the mid-shelf and shelf-break regions even during the winter cruise (GEF-3). Nevertheless, the satellite penetration depth, Z_{pd}, was always shallower than the Z_m in all of the stations except at two stations in the shelf-break sampled during the spring cruise (GEF-1). The good performance of the simplified uniform biomass primary production model used in the present study can be explained considering that production in the water column will become zero when light reaches zero and in most of the stations this occurred before the physical stratification (wherein phytoplankton was usually evenly distributed).

4.2. Primary production using satellite data

The use of ocean color data in primary production models provides an attractive alternative to field estimations, enabling its estimation at high spatial and temporal resolution. In order to make the best use of this technique, an assessment of the accuracy of the satellite-derived products is essential to know the uncertainty of the input data to the models. In a previous work (Dogliotti, Segura, & Lutz, 2010) a sensitivity analysis of the input variables to the BIOM model showed that *Chla* concentration is the most significant source of variability in modeled P_{ZT},
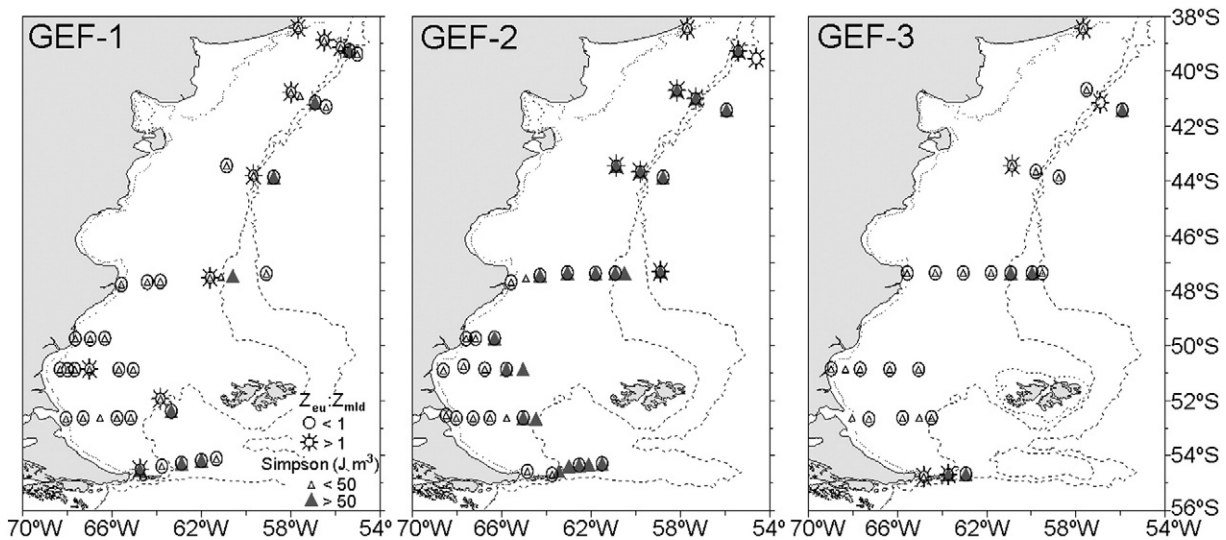
Fig. 7. Distribution of the values of the Simpson parameter (triangles) and Z_{eu}:Z_m (round symbols) during GEF-1 (spring), GEF-2 (summer) and GEF-3 (winter) cruises.

followed by K_d(PAR) and the photosynthetic parameters, and PAR irradiance to a lesser extent. Therefore, when applied to satellite images the main source of uncertainty in P_{ZT} estimates is mainly due to satellite *Chla* estimates which in the present study was ~37% (Table 6), and similar to what was found in this region in a previous work (*bias* approximately −32%, Dogliotti, Schloss, Almandoz, & Gagliardini, 2009). However, a good performance of the BIOM model was found when satellite-derived products and field photosynthetic parameters were used (Fig. 4B and Table 6). This suggests that some of the errors in the satellite-derived inputs may cancel each other. Note that these results were obtained after removing a station where satellite-derived *Chla* highly underestimated the field value. At this station, *Chla* was high, P_{ZT} showed the highest value of all the cruises (19.05 mg m^{-3} and 5477.5 mg C m^{-2} d^{-1}, respectively), and the phytoplankton assemblage was characterized by a bloom condition with the dominance of the diatom *Thalassiosira* cf *oceanica*. A general underestimation (*bias* approximately −30%) and the inability of correctly retrieving *Chla* concentration in this phytoplankton bloom evidences the importance of regionally improving *Chla* satellite estimates.
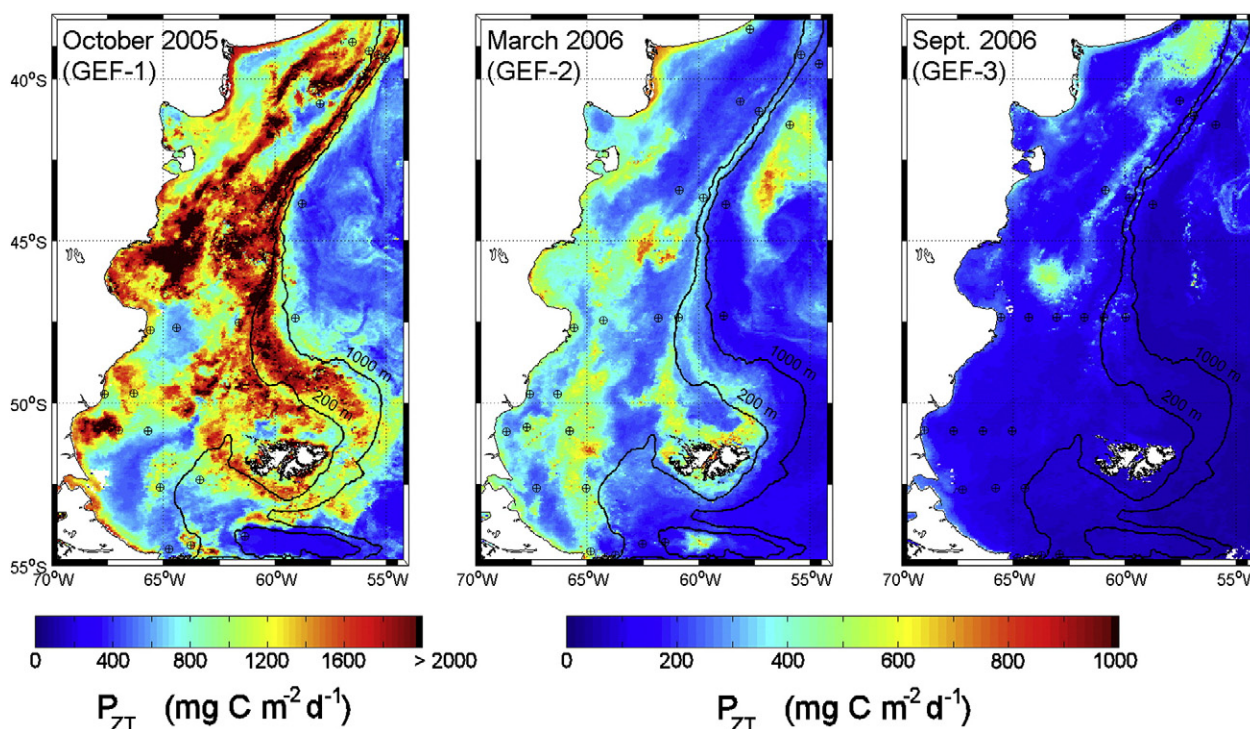
Monthly primary production maps for the three cruises were derived using monthly composites of *Chla*, PAR, K_d(PAR) and average values of the measured photosynthetic parameters corresponding to each cruise homogeneously applied to the whole area of study (Fig. 8). In general, maps of primary production displayed similar features to chlorophyll composite satellite images (Fig. 1): high primary production associated to high *Chla* patches. Primary production values were higher in October 2005 (spring) compared to the other two cruises (note a different scale in Fig. 8), and values in March 2006 (summer) were higher than the values found in September 2006 (winter). However, this monthly maps should be regarded with caution since mean photosynthetic parameters were used while a high variability was found within each cruise.

A first rough estimation of the annual primary production of the continental shelf (<200 m) for 2006 was calculated using the BIOM model. It was applied to satellite-derived monthly composites (from January to December) using the mean photosynthetic parameters found in the present study and applied to each month given its corresponding season. Thus calculated, the annual production for 2006 for the Argentine continental shelf between 38°–55°S was 0.17 Gt y^{-1}. This value was lower than the one estimated by Longhurst, Sathyendranath, Platt, and Caverhill (1995) for the Southwest Atlantic Shelves Province (FLKD) (0.67 Gt y^{-1}) which includes the area of study. It should be noted that the photosynthetic parameters used in our calculations were not significantly different from the ones used by Longhurst given their large variability, but the area therein analyzed was larger (1.42 10^6 km^2) than in the present study (0.93 10^6 km^2), given that the former covered the region east of Malvinas/Falkland islands up to 52°W.

5. Conclusions

We tested five remote sensing based primary production models in the Argentine continental shelf and shelf-break regions using data collected during three cruises in spring 2005, late summer and late winter 2006. The BIOM provided the best estimates of integrated primary production compared to field data (ADP ~10%). The small differences found between BIOM (which assumes uniform biomass profiles) and field estimates (which takes into account the natural vertical distribution of biomass) indicates that in this region and for these analyzed seasons the vertical structure does not play an important role in the estimation of water-column primary production. Reasonable estimates could then be obtained using a simple model that assumes uniform distribution of biological properties with depth. The simplified BIOM also showed a good performance when simultaneous satellite-derived variables and field photosynthetic parameters were used, even though the errors in the satellite-derived data found were around 40%, 20% and 50% for MODIS *Chla*, K_d(PAR), and PAR products, respectively. This result is promising and encourages further investigation on the method for assigning the photosynthetic parameters on a pixel-by-pixel basis, which is the main challenge for this type of models since this information is not accessible by remote sensing. Moreover, the importance of correctly assigning the parameters is clearly evidenced when results from Lutz et al. (2010) and the present study are compared. The BIOM model errors for the spring cruise using fixed values taken from the literature were ~50% (Lutz et al., 2010) while a better performance has been found in the present study when field values were used (~10%). The analysis of different approaches for assigning the photosynthetic parameters is foreseen, which will imply testing methods such as the use of empirical relationships using environmental proxies that can be retrieved from remote sensors (e.g. Bouman et al., 2005), and the use of archived data, either by partitioning the study area into biogeochemical regions (Longhurst et al., 1995) or rearranging them according to *Chla*, SST and day of the year (referred as the nearest-neighbor method, Platt et al., 2008). Clearly, more ship-board observations to help characterize the variability of the parameters and an efficient way to assign them in a pixel-by-pixel basis to obtain reliable estimates of the primary production in this area from remote sensing of ocean color are required.

Fig. 8. Primary production for October 2005, March and September 2006 for the study area derived from monthly composite maps of *Chla*, PAR, K_d(PAR) and mean photosynthetic parameter for each cruise. The sampling locations where *P–I* experiments were performed are superimposed.

Acknowledgements

References

Antoine, D., & Morel, A. (1996). Oceanic primary production 1. Adaptation of a spectral light-photosynthesis model in view of application to satellite chlorophyll observations. *Global Biogeochemical Cycles*, 10(1), 43–55.

Bailey, S., & Werdell, P. (2006). A multi-sensor approach for the on-orbit validation of ocean color satellite data products. *Remote Sensing of Environment*, 102, 12–23.

Banse, K. (1991). Rates of phytoplankton cell division in the field and in iron enrichment experiments. *Limnology and Oceanography*, 36, 1886–1898.

Behrenfeld, M. J., Boss, E., Siegel, D., & Shea, D.M. (2005). Carbon-based ocean productivity and phytoplankton physiology from space. *Global Biogeochemical Cycles*, 19, GB1006. http://dx.doi.org/10.1029/2004GB002299.

Behrenfeld, M. J., & Falkowski, P. G. (1997a). Photosynthetic rates derived from satellite-based chlorophyll concentration. *Limnology and Oceanography*, 42(1), 1–20.

Behrenfeld, M. J., & Falkowski, P. G. (1997b). A consumer's guide to phytoplankton primary productivity models. *Limnology and Oceanography*, 42(7), 1479–1491.

Bertolotti, M. I., Brunetti, N. E., Carreto, J. I., Prenzki, L. B., & Sánchez, R. P. (1996). Influence of shelf-break fronts on shellfish and fish stocks off Argentina. *Int. Con. Exp. Sea, CM 1996/S:41, Theme Session S* (pp. 23).

Bianchi, A., Bianucci, L., Piola, A., Ruiz Pino, D., Schloss, I., Poisson, A., et al. (2005). Vertical stratification and sea–air CO_2 fluxes in the Patagonian shelf. *Journal of Geophysical Research*, 110, C07003. http://dx.doi.org/10.1029/2004JC002488.

Bianchi, A. A., Ruiz Pino, D., Isbert Perlender, H. G., Osiroff, A. P., Segura, V., Lutz, V., et al. (2009). Annual balance and seasonal variability of sea–air CO_2 fluxes in the Patagonian

Sea: Their relationship with fronts and chlorophyll distribution. *Journal of Geophysical Research*, 114, C03018. http://dx.doi.org/10.1029/2008JC004854.

Bouman, H., Platt, T., Sathyendranath, S., & Stuart, V. (2005). Dependence of lightsaturated photosynthesis on temperature and community structure. *Deep-Sea Research I, 52*, 1284–1299.

Campagna, C., Quintana, F., Le Boeuf, B. J., Blackwell, S., & Crocker, D. (1998). Diving behavior and foraging ecology of female southern elephant seals from Patagonia. *Aquatic Mammals*, 24(1), 1–11.

Carr, M. -E., Friedrichs, M.A.M., Schmeltz, M., Aita, M. N., Antoine, D., Arrigo, K. R., et al. (2006). A comparison of global estimates of marine primary production from ocean color. *Deep-Sea Research II, 53*, 741–770.

Carreto, J. I., Carignan, M.O., Montoya, N. G., & Cuchi-Colleoni, A.D. (2007). Ecología del fitoplancton en los sistemas frontales del Mar Argentino. In J. I. Carreto, & C. Bremec (Eds.), *El Mar Argentino y sus recursos pesqueros. El ecosistema marino, Tomo 5*. (pp. 11–31). Mar del Plata, Argentina: Inst de Invest. y Desarrollo Pesq. INIDEP.

Claustre, H., Babin, M., Merien, D., Ras, J., Prieur, L., & Dallot, S. (2005). Toward a taxonspecific parameterization of bio-optical models of primary production: A case study in the North Atlantic. *Journal of Geophysical Research*, 110, C07S12.

Cullen, J. J. (1990). On models of growth and photosynthesis in phytoplankton. *Deep-Sea Research*, 37, 667–683.

Dogliotti, A. I., Schloss, I. R., Almandoz, G. O., & Gagliardini, D. A. (2009). Evaluation of SeaWiFS and MODIS chlorophyll-*a* products in the Argentinean Patagonian Continental Shelf (38°S–55°S). *International Journal of Remote Sensing, 30*, 251–273.

Dogliotti, A. I., Segura, V., & Lutz, V. A. (2010). Primary production in the Patagonian Continental Shelf and shelf-break region: Improved estimation using satellite-based models. *Proceeding of Ocean Optics XX Conference, Paper No. 100850, Anchorage, Alaska. 27 Sept.–1 October, 2010* (12 pp.).

Dogliotti, A. I., Segura, V., & Lutz, V. A. (2012). Assessing satellite-derived variables used in primary production models in the Argentine Sea. *Proceeding of Congreso Argentino de Teledeteccion 2012: El medio ambiente y sus cambios: un desafío para la información espacial (CAT-2012), paper no. OO01, Ciudad de Córdoba, Argentina. 18–21 September, 2012* (5 pp.).

El-Sayed, S. Z. (1967). On the productivity of the Southwest Atlantic Ocean and the waters west of the Antarctic Peninsula. In W. Schmitt & G.A. Llano (Eds.), *Biology of the Antarctic Seas III. Antarctic Research Series, 11.* (pp. 15–47). Washington: American Geophysical Society.

Eppley, R. W. (1972). Temperature and phytoplankton growth in the Sea. *Fishery Bulletin*, 79(4).

Eppley, R., Steward, E., Abbott, M., & Heyman, U. (1985). Estimating ocean primary production from satellite chlorophyll: Introduction to regional differences and statistics for the Southern California Bight. *Journal of Plankton Research*, 7, 57–70.

Forget, M. -H., Sathyendranath, S., Platt, T., Pommier, J., & Fuentes-Yaco, C. (2007). Computation of primary production from remote-sensing of ocean colour of the lagrangian site of C-SOLAS. *Marine Ecology Progress Series, 352*, 27–38.

Garcia, V. M. T., Garcia, C. A. E., Mata, M. M., Pollery, R. C., Piola, A., Signorini, S. R., et al. (2008). Environmental factors controlling the phytoplankton blooms at the Patagonia shelf-break in spring. *Deep-Sea Research I, 55*, 1150–1166.

Gómez, M. I., Piola, A., Katter, G., & Alder, V. A. (2011). Biomass of autotrophic dinoflagellates under weak vertical stratification and contrasting chlorophyll levels in subantarctic shelf waters. *Journal of Plankton Research — Short Communication, 33*, 1304–1310.

Hama, T., Miyazaki, T., Ogawa, Y., Iwakuma, T., Takahashi, M., Otsuki, A., et al. (1983). Measurement of photosynthetic production of a marine phytoplankton population using a stable ^{13}C isotope. *Marine Biology, 73*, 31–36.

Hoepffner, N., & Sathyendranath, S. (1992). Bio-optical characteristics of coastal waters: Absorption spectra of phytoplankton and pigment distribution in the western North Atlantic. *Limnology and Oceanography, 8*, 1660–1679.

Holm-Hansen, O., Lorenzen, C. J., Holmes, R. W., & Strickland, D. H. (1965). Fluorometric determination of chlorophyll. *Conseil International pour l'Exploration de la Mer, 30*, 3–15.

Kiefer, D. A., & Mitchell, B. G. (1983). A simple, steady state description of phytoplankton growth based on absorption cross section and quantum efficiency. *Limnology and Oceanography, 28*, 770–776.

Lee, Z. P., Carder, K. L., Marra, J., Steward, R. G., & Perry, M. J. (1996). Estimating primary production at depth from remote sensing. *Applied Optics, 35*, 463–474.

Lee, Z. P., Weidemann, A., Kindle, J., Arnone, R., Carder, K. L., & Davis, C. (2007). Euphotic zone depth: Its derivation and implication to ocean-color remote sensing. *Journal of Geophysical Research, 112*, C03009. http://dx.doi.org/10.1029/2006JC003802.

Longhurst, A., Sathyendranath, S., Platt, T., & Caverhill, C. (1995). An estimate of global primary production in the ocean from satellite radiometer data. *Journal of Plankton Research, 17*, 1245–1271.

Lutz, V. A., Segura, V., Dogliotti, A. I., Gagliardini, D. A., Bianchi, A. A., & Balestrini, C. F. (2010). Primary production in the Argentine Sea during spring estimated by field and satellite models. *Journal of Plankton Research, 32*(2), 181–195. http://dx.doi.org/10.1093/plankt/fbp117.

Mandelli, E. F. (1965). Contribución al conocimiento de la producción orgánica primaria en aguas Sub-Antárticas (Océano Atlántico Sud-Occidental). *Anais da Academia Brasileira de Ciências, 37*, 399–407.

Maritorena, S., Siegel, D. A., & Peterson, A. (2002). Optimization of a semi-analytical ocean color model for global scale applications. *Applied Optics, 41*(15), 2705–2714.

Marra, J., Ho, C., & Trees, C. (2003). *An Alternative Algorithm for the Calculation of Primary Productivity From Remote Sensing Data, LDEO Tech. Rep. DEO-2003–DEO-1.* New York, N. Y.: Lamont-Doherty Earth Observ. Of Columbia Univ.

Marra, J., Trees, C. C., & O'Reilly, J. E. (2007). Phytoplankton pigment absorption: A strong predictor of primary productivity in the surface ocean. *Deep Sea Research I, 54*(2), 155–163. http://dx.doi.org/10.1016/j.dsr.2006.12.001.

Martos, P., & Piccolo, M. C. (1988). Hydrography of the Argentine Continental-shelf between 38°S and 42°S. *Continental Shelf Research, 8*(9), 1043–1056.

Mitchell, B. G. (1990). *Algorithms for Determining the Absorption Coefficient of Aquatic Particulates Using the Quantitative Filter Technique (QFT).* Orlando, Florida: SPIE, Ocean Optics X.

Negri, R. M. (1993). *Fitoplancton y producción primaria en el área de la plataforma bonaerense próxima al talud continental, 1.* (pp. 1–7): INIDEP Informe Tecnico, 1–7.

Platt, T., Forget, M. -H., White, G., Son, S., Bouman, H. A., Devred, E., et al. (2008). Operational mode estimation of primary production at large geographical scales. *Remote Sensing of Environment, 112*, 3437–3448.

Platt, T., Gallegos, C. L., & Harrison, W. G. (1980). Photoinhibition of photosynthesis in natural assemblages of marine phytoplankton. *Journal of Marine Research, 38*, 687–701.

Platt, T., & Sathyendranath, S. (1988). Oceanic primary production: Estimation by remote sensing at local and regional scales. *Science, 241*, 1613–1620.

Reta, R. (2009). Delimitación de la profundidad de la capa de mezcla en la plataforma patagónica austral. *Campañas GEF I, II y III. VII Jornadas Nacionales de Ciencias del Mar, Bahía Blanca, Buenos Aires, Argentina. 30 November–4 December, 2009.*

Rivas, A. L., Dogliotti, A. I., & Gagliardini, D. A. (2006). Seasonal variability in satellite-measured surface chlorophyll in the Patagonian shelf. *Continental Shelf Research, 26*, 703–720.

Romero, S. I., Piola, A.R., Charo, M., & Garcia, C. A. E. (2006). Chlorophyll-*a* variability off Patagonia based on SeaWiFS data. *Journal of Geophysical Research, 111*, C0521. http://dx.doi.org/10.1029/2005JC003244.

Sabatini, M., Akselman, R., Reta, R., Negri, M. R., Lutz, V. A., Silva, C., et al. (2012). Spring plankton communities in the southern Patagonian shelf: Hydrography, mesozooplankton patterns and trophic relationships. *Journal of Marine Systems, 94*, 33–51.

Sathyendranath, S., & Platt, T. (1988). The spectral irradiance field at the surface and in the interior of the ocean: A model for applications in oceanography and remote sensing. *Journal of Geophysical Research, 93*, 9270–9280.

Sathyendranath, S., & Platt, T. (1993). Remote sensing of water-column primary production. In W. K. W. Li, & S. Y. Maestrini (Eds.), *Measurement of Primary Production From the Molecular to the Global Scale* (pp. 236–243). Copenhagen: ICES.

Schloss, I. R., Ferreyra, G. A., Ferrario, M. E., Almandoz, G. O., Codina, R., Bianchi, A. A., et al. (2007). Role of phytoplankton communities in the sea–air variation of pCO$_2$ in the SW Atlantic Ocean. *Marine Ecology Progress Series, 332*, 93–106.

Segura, V., Lutz, V. A., Dogliotti, A. I., Silva, R., Negri, R., Akselman, R., et al. (2013). Phytoplankton Types and primary production in the Argentine Sea. *Marine Ecology Progress Series, 491*, 15–31.

Son, S., Campbell, J., Dowell, M., Yoo, S., & Noh, J. (2005). Primary production in the Yellow Sea determined by ocean color remote sensing. *Marine Ecology Progress Series, 303*, 91–103.